IJST, Transactions of Mechanical Engineering, Vol. 39, No. M2, pp 399-412
Printed in The Islamic Republic of Iran, 2015

EXPERIMENTAL AND NUMERICAL INVESTIGATION OF THE EFFECT OF DIMPLE AND PERFORATIONS ON NUSSELT NUMBER AND FLOW EFFICIENCY IN MULTI-LOUVERED HEAT EXCHANGER*

H. SHOKUHMAND AND F. SANGTARASH**

Dept. of Mechanical Engineering, University of Tehran, Tehran, I. R. of Iran
Email: f.sangtarash@ut.ac.ir

Abstract– Numerical and experimental analyses are performed on multilouvered fin banks in low and medium Reynolds regimes to investigate the effects of dimples and perforations on flow structure and heat transfer capacity. In different Reynolds numbers the flow efficiency has been calculated numerically and experimentally by flow visualization method and the results showed that dimples and perforations can increase flow efficiency more than 5% in fin banks. Additionally, a set of numerical and experimental analysis has been done to evaluate temperature contours and total heat transfer in simple, dimple and dimple-perforation fin banks in different Reynolds Numbers. The simulations revealed that the heat transfer and temperature augmentations occur due to the existence of a circulation region that is created by the dimple. The results showed that adding dimples with perforations increased the heat transfer capacity of the fin banks up to 9% compared with the simple louver fin banks.

Keywords– Multilouvered fin, dimple, perforation, flow efficiency, heat transfer enhancement

1. INTRODUCTION

The variety of applications of heat exchangers in several industries such as thermal processing systems in automotive, HVAC, refrigeration has made it necessary to enhance their performance. The commonly applicable way to improve the overall performance of the compact heat exchanger is to use interrupted surfaces on the fin side [1, 2]. One of the most widely used designs among interrupted surfaces is the multilouvered geometry. In the past decades many experimental and numerical studies have been conducted to demonstrate the flow characteristics [3, 4].

Beauvias [5] was the first to perform flow visualization experiments on the louvered fin array. He showed that louvers actually redirect the flow between the fins. Flow visualization performed by Davenport [6] demonstrated two asymptotic flow regimes; duct directed flow, and louver directed flow. In the former the predominant flow is streamwise while in the latter the predominant flow is aligned with the louvers. Zhang and Tafti [7] showed that the flow direction has significant implications for the overall heat capacity of the fin because of its strong effect on the heat transfer coefficient. A parameter called flow efficiency was defined as the degree to which the flow is aligned to the louver direction to be able to quantify the flow regime [7, 8]. Zhang and Tafti [9] showed that high flow efficiency enhances the heat transfer coefficient. They studied the effects of intra-fin and inter-fin thermal wakes on the heat transfer capacity of the fin array. They suggested that thermal wake effects can be expressed as functions of the flow efficiency and the fin pitch-to-louver pitch ratio [9].

*Received by the editors December 3, 2014; Accepted May 13, 2015.
**Corresponding author

Zhang *et al.* [10, 11] and Tafti *et al.* [12, 13] have studied the effects of flow oscillations in the form of large-scale vorticity on the heat transfer coefficient. Tafti *et al.* [13] investigated the transition from steady laminar to unsteady flow in a multilouvered fin array. The local heat transfer from the fin surface was found to be strongly affected by the large-scale vortices shed from the louver.

Afansayev *et al.* [14] studied the effects of shallow dimples on flat plates on the overall heat transfer capacity and pressure drop. They reported a significant heat transfer enhancement (30-40 %) at a low pressure drop cost.

Ligrani *et al.* [15, 16] experimentally investigated the flow structure in dimpled surfaces and showed the existence of flow recirculation zone in the upstream half of the dimples. A region of low heat transfer was observed in the upstream half of the dimple cavity followed by a high heat transfer region in the flow reattachment region in the downstream half of the dimple and the flat landing downstream of the dimple [16, 17].

Zhengyi *et al.* [18] observed a symmetric 3-D horseshow vortex inside a single dimple using laminar flow simulations. Flow structure and heat transfer in dimpled channel in fully turbulent regimes were studied in the literature. Large eddy simulation (LES) and direct numerical simulation (DNS) have largely been used by several researchers in order to study the fluid flow and heat transfer in heat exchangers [16, 17].

This paper experimentally and numerically investigates the effect of fin geometry, which includes simple louver, dimpled louver, and dimpled-perforation louver on heat transfer in multilouvered heat exchangers. In order to properly investigate the flow and heat transfer characteristics, LES method is used to model the low Reynolds turbulence flow. The computational results are compared with data obtained from experiments. The flow efficiency is calculated to evaluate its effects on the heat transfer augmentation. The experimental data shows the enhancement of the heat transfer by applying dimpled louver and dimpled-perforation louver fin banks.

2. METHOD

a) Computational details

The momentum and energy equations were solved using second-order central-difference discretization. The commercial package Fluent 6.3 [17] was used to simulate the computational three-dimensional models. Three geometries have been modeled to obtain the results for the CFD predictions. We have studied low and medium Reynolds number regimes (Re = 200 to 1000) using large eddy simulation (LES) methods. Previous studies [16, 22] have explained that the LES method is more capable for complex geometrical configurations. A suitable grid of 2,151,382 points was adopted to obtain the most accurate results while being less time consuming for convergence. One half of the fin height has been modeled for the numerical calculations, and the results for the other half are gained by specifying a symmetric boundary condition along the middle surface of the entire domain. The inlet velocity upstream and the outflow velocity downstream of the louvers have been set as boundary conditions. The constant temperature boundary condition has been imposed on the wall at the base of the louvers. Figure 1a shows the multilouvered fin array while Fig. 1b shows the computational unit consists of only one row of louvers. Periodic boundary conditions are applied in transverse direction in order to include the thermal wake effects between successive rows of fins. Dirichlet boundary condition is applied to velocity and temperature fields at the entrance of the array.

Fig. 1.

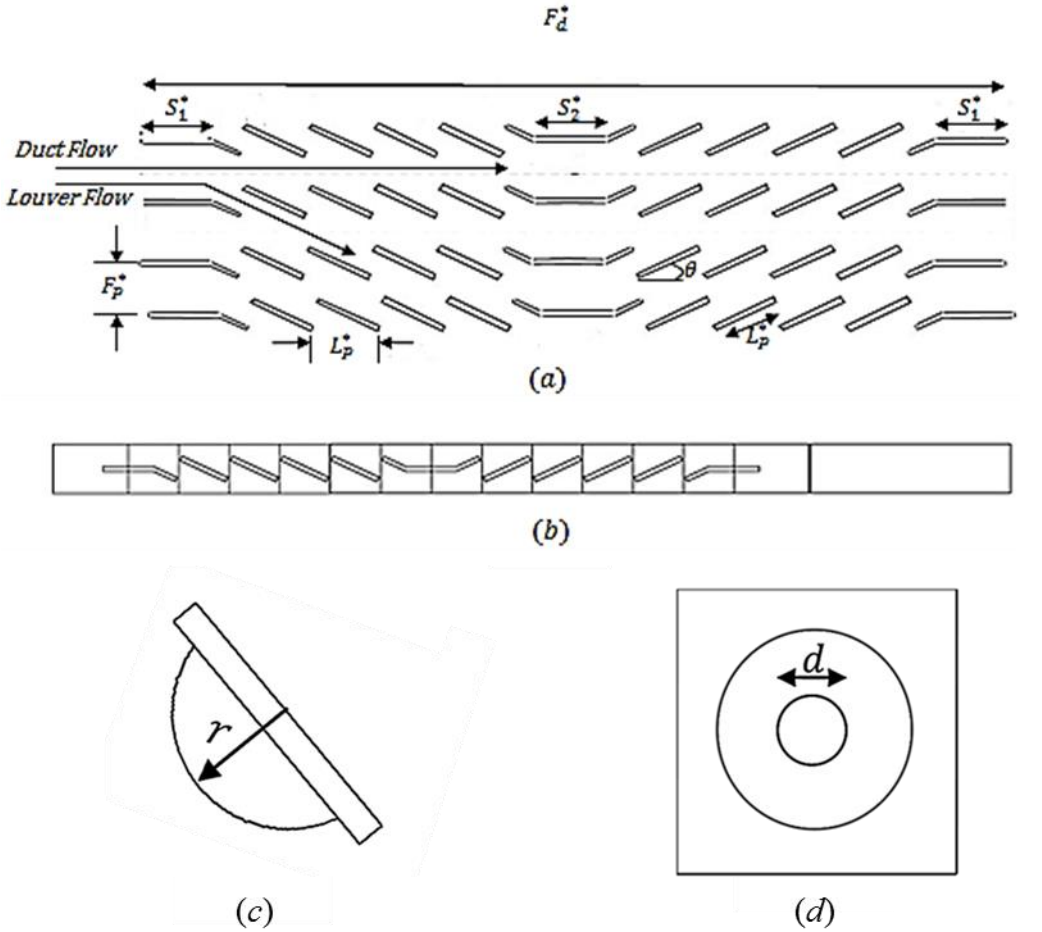

Fig. 1. (a) Multilouvered fin geometry (b) numerical analysis domain (c) an individual dimpled louver (d) perforated dimpled louver layout

The fin array geometry used in these calculations consists of an entrance and exit louver with four louvers on either side of the redirection louver. For all the calculations in this article, louver thickness is fixed at 0.1 mm. Further geometrical details are listed in Table 1.

Table 1. List of geometrical parameters

Case	F_p^*	L_p^*	θ	S_1^*	S_2^*	r	d
Simple Louver	10.0 mm	10.0 mm	30°	8.0 mm	10.0 mm	-	-
Dimpled Louver	10.0 mm	10.0 mm	30°	8.0 mm	10.0 mm	6.0 mm	-
Perforated Louver	10.0 mm	10.0 mm	30°	8.0 mm	10.0 mm	6.0 mm	2.5 mm

In this article the governing equations are non-dimensionalized by a characteristic length, the louver pitch L_P^*, a characteristic velocity, the inlet velocity to the array of fins u_{in}^* and a temperature scale given by (T_f^*- T_{in}^*), where T_f^* is the louver surface temperature. No slip and no penetration conditions for the velocity field and no temperature jump for temperature field are applied on the louvers surfaces. The non-dimensionalization would result in a Reynolds number defined by $\mathrm{Re} = \mathrm{Re}_{in} = u_{in}^* L_p^* / \nu$ and Dirichlet boundary condition $u_{in}= 1$ and $T_{in} = 0$ at the entrance of the array. The Prandtl number is fixed at 0.7 for air. Patrick and Tafti [19] suggested that LES method can be used to study the low Reynolds turbulence flows in multilouvered geometries. DeJong and Jacobi [20] suggested that for similar multilouvered array layout for low Reynolds numbers the flow is steady and laminar. As the Reynolds number is increased to approximately 500, small-scale periodic transverse velocity functions generated upstream propagate downstream and the louvers between the redirection louver and the exit louver start to shed small

spanwise vortices. Higher Reynolds flow leads to larger vortices and changes the flow from laminar to transition and turbulent regimes.

b) Characterization of heat transfer

It is best to describe the relationship between dimensional and non-dimensional parameters used to study the heat transfer. The dimensional heat flux on the louver surface is defined as

$$q^* = -k\frac{\partial T^*}{\partial n^*} = h^*(T_f^* - T_{ref}^*) \tag{1}$$

where n^* is along the normal vector to the louver surface, and T_{ref}^* is the dimensional flow reference temperature. Using the non-dimensionalized variables the above equation is expressed as

$$q^* = -\frac{k}{L_p^*}(T_f^* - T_{in}^*)\frac{\partial T}{\partial n} = h^*(T_f^* - T_{in}^*)(1 - T_{ref}) \tag{2}$$

The non-dimensional heat flux and Nusselt number can be defined as

$$q = \frac{q^* L_p^*}{k(T_f^* - T_{in}^*)} = -\frac{\partial T}{\partial n} \tag{3}$$

$$Nu = \frac{h^* L_p^*}{k} = \frac{-\frac{\partial T}{\partial n}}{(1 - T_{ref})} \tag{4}$$

In this article T_{ref} is calculated by the log-mean temperature equation:

$$T_{ref} = 1 - \frac{T_{out} - T_{in}}{\ln(\frac{1 - T_{in}}{1 - T_{out}})} \tag{5}$$

For each louver, T_{ref} is calculated using each computational input and output data. T_{in} and T_{out} are averaged on the upstream and downstream boundary of each louver respectively.

c) Flow characteristics

The flow direction, which is quantified by flow efficiency, has significant implication on the overall heat transfer capacity of the fin array mainly because of its strong effect on the heat transfer coefficient. The flow efficiency is calculated as α_{mean}/θ, where α is the flow angle and θ is the louver angle. The flow angle for each louver can be obtained individually based on $\alpha = \tan^{-1}(\frac{m_y}{m_x})$ where $m_y = \int v dx$ and $m_y = \int u dy$ are the average mass flow rates calculated at the top and left face of each louver. Flow efficiency is then defined as the ratio of mean flow angle which is the average flow angle throughout louvers 2-5 and 7-10 (entrance, redirection and exit louvers are excluded) to louver angle. Whereas in experimental dye injection studies, the flow efficiency is calculated as the ratio of actual transverse distance *N* traveled by the dye to the ideal distance *D* (Fig. 2).

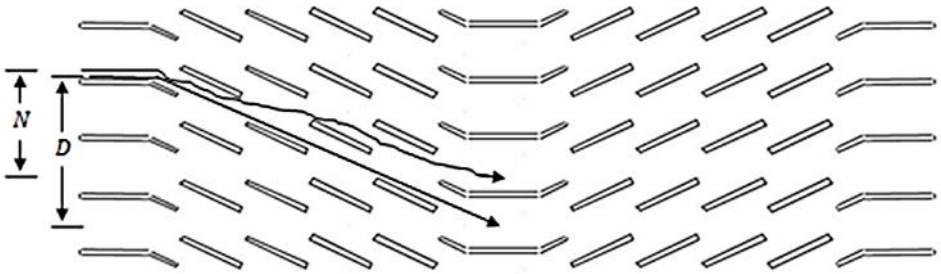

Fig. 2. Definition of experimental flow efficiency as $\eta=N/D$

d) Experimental apparatus

A low turbulence wind tunnel, Model No.TE.44/D Manufactured by PLINT and PARTNERS ENGINEERS LTD, has been used in this research. The cross section of measurement part is 460×460 mm and the length of the test section is 600 mm. The non-uniformity of velocity distribution is negligible. The turbulence intensity is less than 0.2 for the maximum Reynolds number in our test domain. The experiment apparatus is shown in Fig. 3.

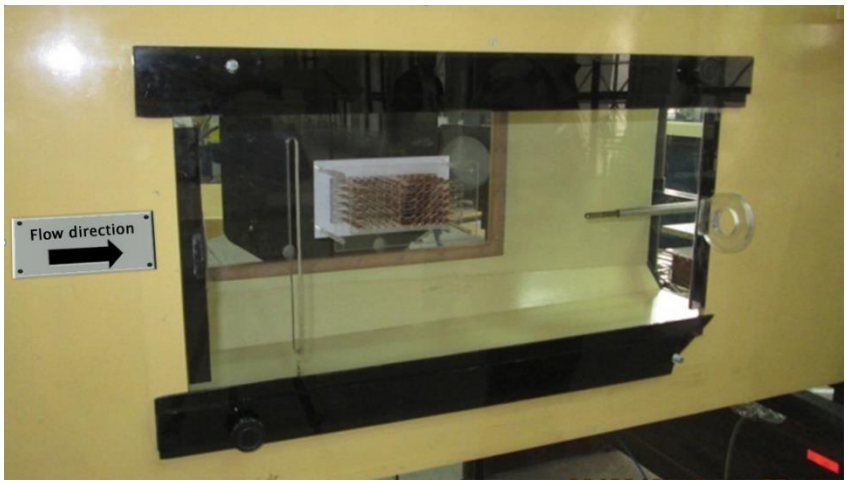

Fig. 3. Experimental apparatus

e) Sample Models

A scaled-up (ratio of 10) inclined louvered fin model was used as simple model. Additionally, two samples, including dimples and perforated dimples, were constructed with the same size. Dejoy and Jacobi presented a calculation method to find the minimum required rows of fins for flow visualization studies without losing periodic. This method has been used in this research and the smoke has been injected at a specific point in the upstream of the test section to visualize the flow.

f) Temperature data gathering

A temperature controller circuit was designed to maintain the temperature at 100°C to maintain a constant temperature condition at both sides of each louver. The controller will verify the temperature 20 times per second to achieve a minimum deviation from the setpoint. An energy meter with high resolution and accuracy of 0.1 W was used to verify that energy is consumed to set the temperature of both sides of each louver to the setpoint value. A data gathering system was designed to make online measurement of the temperature. The temperatures from seven zones on the surface of different louvers have been measured using thermal sensors with an accuracy of 0.2 °C in the different Reynolds numbers. All values were recorded when the temperature of the measurement zone stabilized.

3. RESULTS AND DISCUSSION

a) Simulation accuracy verification

To begin discussing the results of the various geometries we must first verify the accuracy of the model with one existing set of data. Here, we used the report by Zhang and Tafti [9] on simple multilouvered geometry.

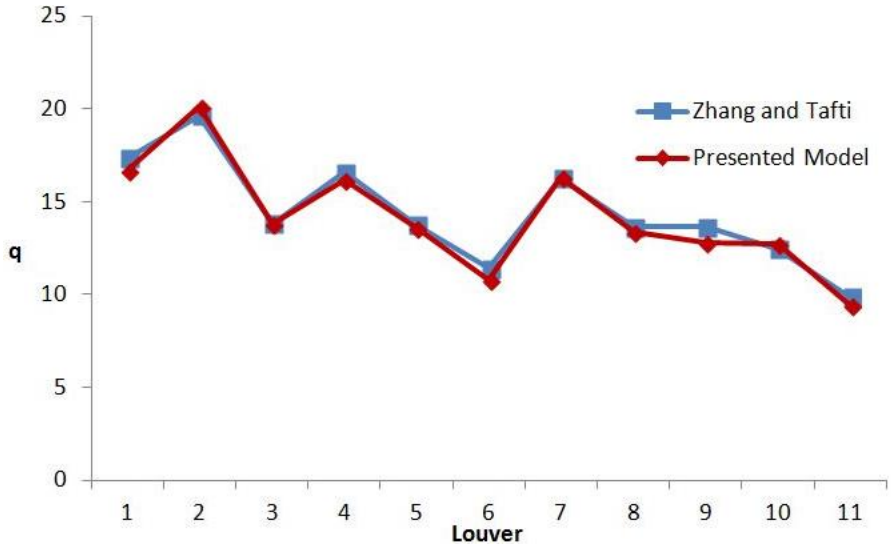

Fig. 4. Comparison of non-dimensional heat flux distribution on louver basis

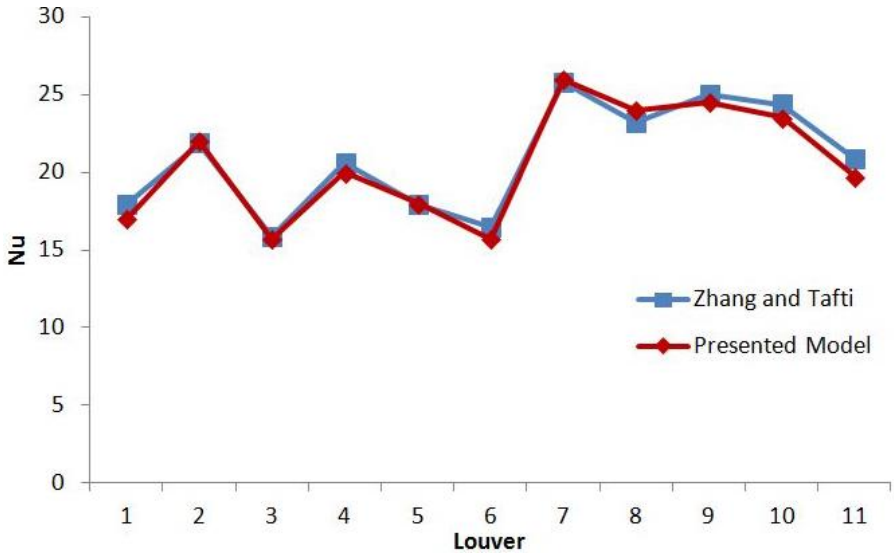

Fig. 5. Comparison of Nusselt number distribution on louver basis

Figures 4 and 5 present the non-dimensional heat flux distribution and Nusselt number distribution through louvers based on data from Zhang and Tafti [9] and the presented model for simple multilouvered geometry with Re = 1000. The data sets are observed to be approximately the same (less than 5% deviation). The flow efficiency, which is calculated from the presented model, has less than 1% deviation from the Zhang and Tafti [9] data.

b) Computational

Flow and heat transfer characteristics are discussed in simple, dimpled and perforated louvered fin configurations for various Re numbers (Re = 200 to 1000) using large eddy simulation (LES) methods. Figure 6 shows flow efficiencies for these geometries. It is shown that the calculated flow efficiency

increases for dimpled and perforated geometries in comparison with simple louvered geometry for the same Re numbers.

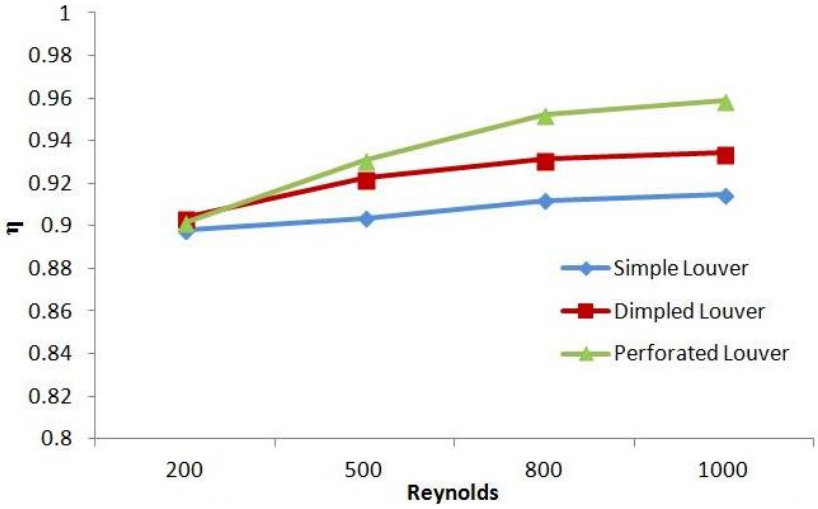

Fig. 6. Numerical flow efficiency for three geometries

Tafti and Zhang [9] classified two primary mechanisms, intra-fin interference and inter-fin interference, in which the louvers thermally interfere with each other. The intra-fin interference is dominant in duct directed flows where the thermal wakes of upstream louvers interfere with successive downstream ones. The inter-fin interference is dominant in louver directed flows where thermal wakes between fin rows interfere with each other. The intra-fin and the inter-fin thermal wake interferences can be seen in Fig. 7. It should be noted that both types of interferences occur in the same time but their dominancy is strongly dependent on flow efficiency. The 3D contour of the temperature distribution for a dimpled louver is illustrated in Fig. 8. According to Fig. 8, the temperature of the louvers increased in the direction of the fluid flow. This is due to the fact that, the heat is transferred from the louvers to the fluid which makes the temperature of the louvers higher and higher in the direction of the fluid flow. Moreover, it can be observed that the temperature of each louver decreases from the base to the center regions of the louvers.

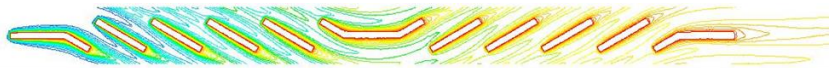

(a) simple louver, Re = 1000

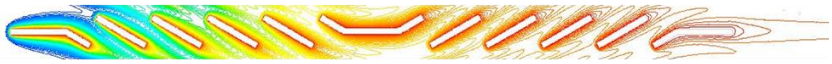

(b) simple louver, Re = 200

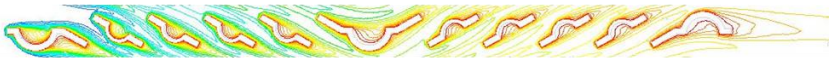

(c) dimpled louver, Re = 1000

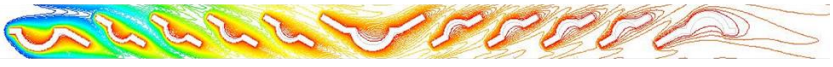

(d) dimpled louver, Re = 200

(e) dimpled-perforation louver, Re = 1000

(f) dimpled-perforation louver, Re = 200

Fig. 7. Temperature contours with thermal wake effects

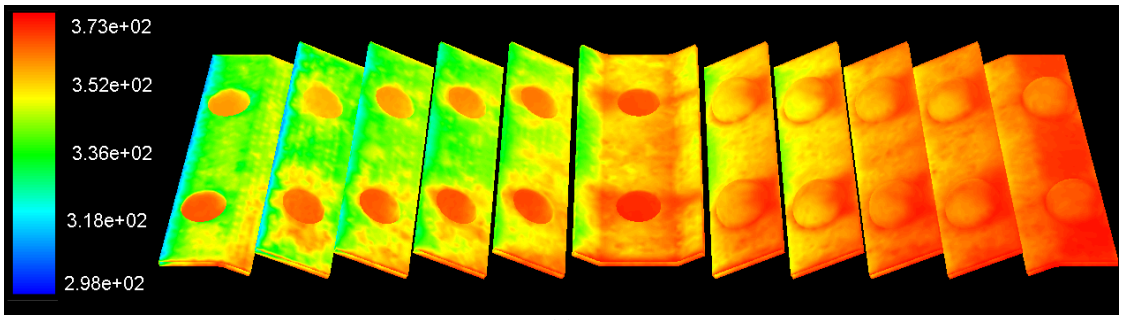

(a)

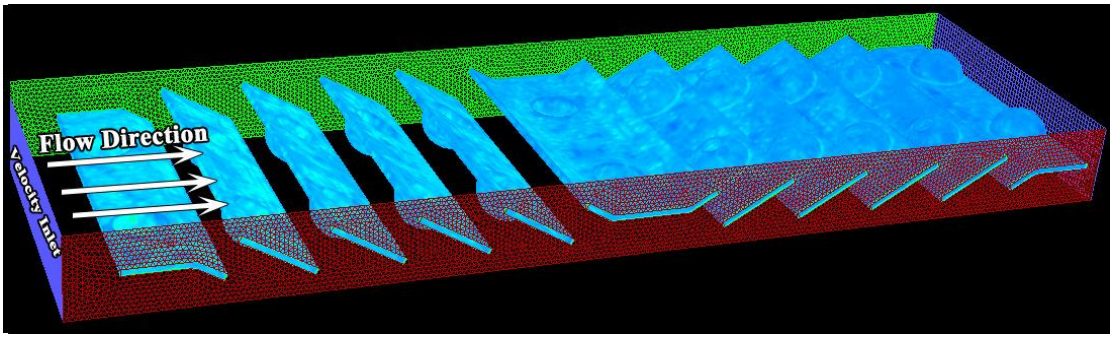

(b)

Fig. 8. a) Temperature (K) contours for a dimpled louver in Re = 600 b) Louver boundary condition

Figure 9 plots variation of the non-dimensional heat flux on a louver by louver basis for three different geometries. In Fig. 9a, the heat flux decreases continuously towards the downstream in a way that only a small portion of the total louver array heat transfer is from louvers downstream of the re-direction louver (louver number 6). This behavior is because of the thermal saturation and the effects of intra-fin thermal wake interferences. In higher Re regimes, the flow is more louver directed, hence the heat flux variation is not as sharp as it is in low Re regimes.

Fig. 9

Figure 9b shows that in larger Reynolds number, the heat fluxes of the upstream louvers are higher for perforated dimpled louvers while on the downstream of the re-direction louver the stronger inter-fin thermal wake interferences cause the heat flux to decrease. In smaller Reynolds number the thermal saturation effect is dominant and hence all three cases act similarly.

Nusselt number variation on a louver by louver basis is presented in Fig. 10. In perforated louver case, for Re = 1000, the average of Nu values are mostly higher than the simple louver. The entrapped flow in the dimple cavity increases the fluid temperature and leads to higher reference temperature and higher heat transfer coefficient. Implying dimples on the louver surface leads to the total heat transfer rate augmentation at a constant velocity (constant Re number).

c) Experimental results

Figure 11 shows the result of visual flow efficiency for different cases for Re=1000. Fig. 12a presents the experimental flow efficiencies for various Re numbers for three cases. The overall trend of these data is similar than calculated flow efficiencies, which had been presented in Fig. 6. Figures 12b to 12d compare the results of visual test flow efficiencies with numerical results. The maximum deviation between experimental and numerical results is about 5% in different Reynolds number.

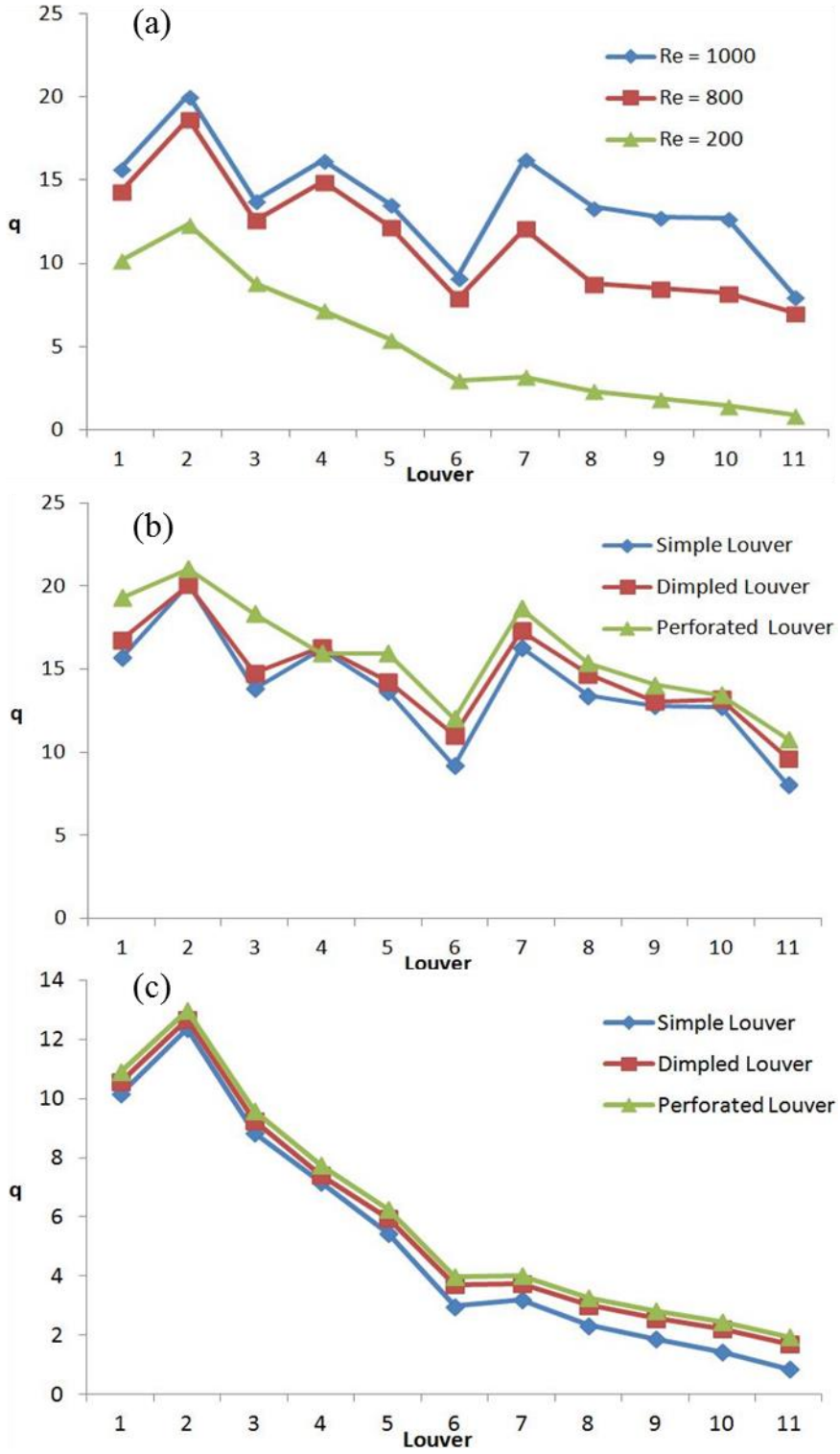

Fig. 9. Distribution of non-dimensional heat flux (a) simple louver (b) Re = 1000 (c) Re = 200

Figure 13 presents the total heat transfer energy ratio for dimpled and dimpled-perforation samples compared with the simple louver case. These measurements were obtained using the energy meter from the experimental apparatus at different Reynolds numbers.

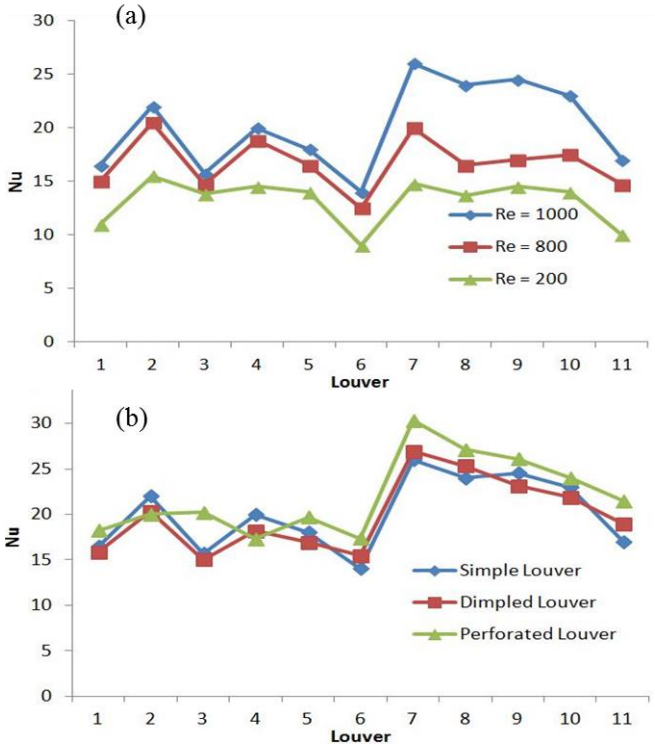

Fig. 10. Distribution of Nusselt number for (a) simple louver and for (b) Re = 1000

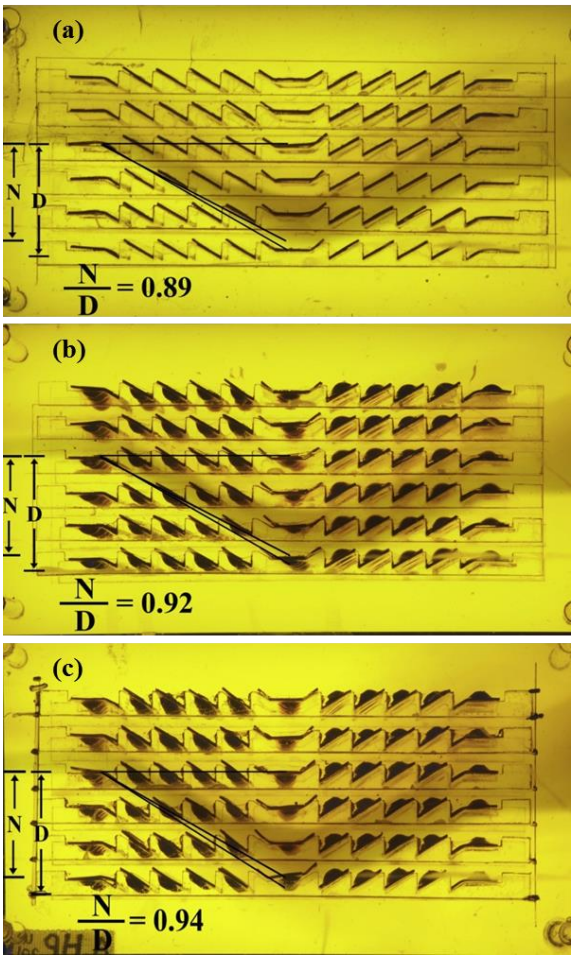

Fig. 11. Experimental flow efficiency (a) simple louver (b) dimpled louver (c) dimpled-perforation louver

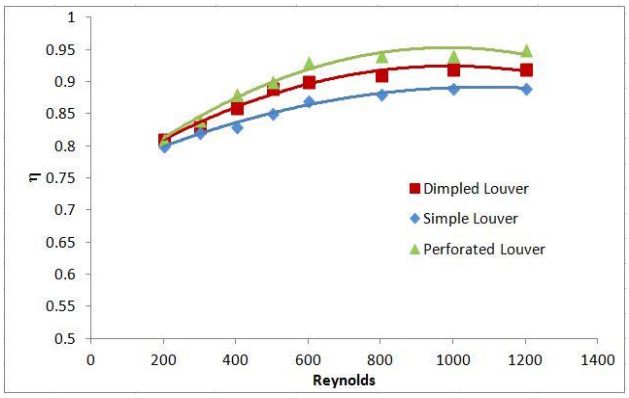

(a)

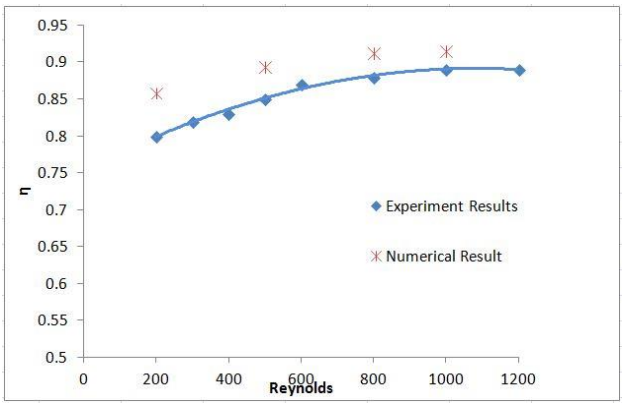

(b)

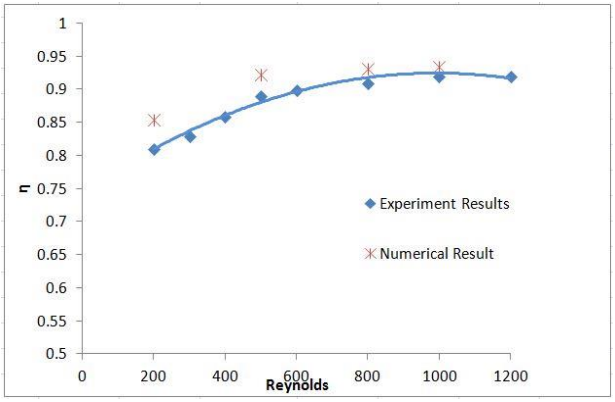

(c)

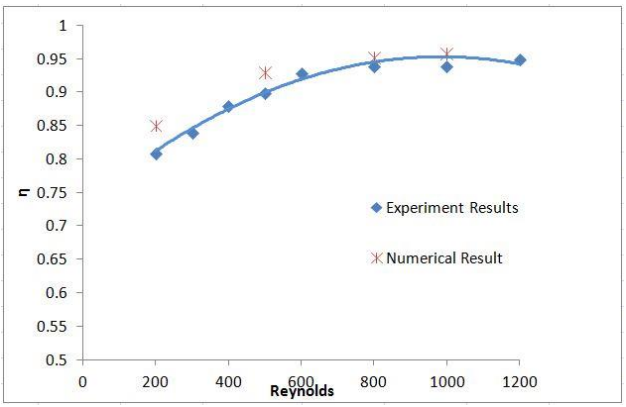

(d)

Fig. 12. (a) Experimental flow efficiency and comparison of the flow efficiency between numerical and experimental results in (b) simple louver (c) dimpled louver (d) dimpled-perforation louver

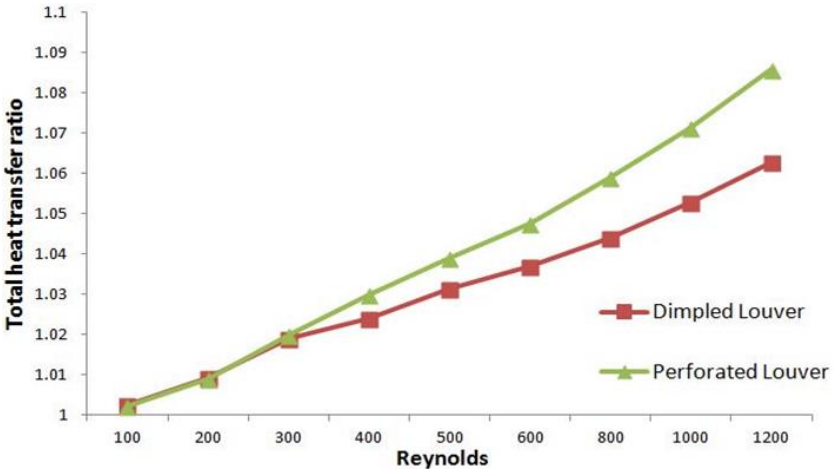

Fig. 13. Total heat transfer ratio compared with the simple louver case

It can be observed from Fig. 12 that the total heat transfer for dimpled and dimpled-perforation cases, which has been measured during the experiment, are nearly the same for low Reynolds numbers, but the heat transfer changes for higher Reynolds numbers. Figure 12 shows that the total heat transfer is 6.5% and 9% greater than the simple louver geometry for dimpled and dimpled-perforation cases for a Re number of 1200, respectively.

4. UNCERTAINTY ANALYSIS

Uncertainty of each experimental result is one of the most important factors that makes the results more comprehensive. These uncertainties are affected by inevitable errors occurring in the experimental measurements which can be linked to the uncertainty of individual measuring instruments.

Based on the uncertainty analysis method of Kline and McClintock [21], propagation of uncertainty in the final result is affected by the uncertainties of independent variables. This method is employed to estimate the uncertainties of experimental results. The maximum uncertainties of Nusselt number is about 2.4%. It can be concluded from this research work that the calculated values of Nusselt number cover a range of possible values based on the uncertainty of Nusselt number. In addition, it should be noted that all the experiments have been repeated three times in order to have a more reliable result and to be assured of the reproducibility.

5. CONCLUSION

A wide range of numerical and experimental evaluations were performed for three cases, simple louver fin bank, dimpled louver fin bank and dimpled-perforation fin bank. Both the numerical and the experimental results show that dimple-perforation sets increased the flow efficiency and the total heat transfer rate in different Reynolds numbers, which was especially noticeable in larger Reynolds numbers. It was observed from the experimental and numerical calculations that the flow efficiency was increased more than 5 % in fin banks by the implementation of the dimples and perforations. Experimental data showed that applying dimple-perforation geometry enhanced the heat transfer rate up to 6%, 7.2%, and 9% with Reynolds numbers of 800, 1000, and 1200, respectively, compared with the simple louver geometry. The 3D temperature contour manifested that the temperature of the louvers increased in the direction of the fluid flow, while the temperature of the louver decreased from the louver base across the louver. The maximum uncertainty of the Nusselt number was found to be 2.4 % which indicates that the calculated values of Nusselt numbers cover a range of possible values.

NOMENCLATURE

C_p	specific heat capacity
d	hole size
F_p^*	fin pitch
h	heat transfer coefficient
k	thermal conductivity
L_p^*	dimensional louver pitch (characteristic length scale)
Nu	Nusselt number
Pr	Prandtl number
q	non-dimensional heat flux
r	dimple radius
Re	Reynolds number
S_1, S_2	non-dimensional entrance / exit and redirection louver dimensions
T	Temperature
u_{in}^*	dimensional inlet velocity (characteristic velocity scale)
u,v	non-dimensional velocity vector components

Greek Symbols

α	flow angle
η	flow efficiency
θ	louver angle
v	kinematic viscosity

Superscripts

*	dimensional quantities

Subscripts

f, fin	based on fin
in	based on inlet
out	based on outlet
ref	based on reference value

REFERENCES

1. Sohankar, A. (2010). Heat transfer and fluid flow through a ribbed passage in staggered arrangement. *Iranian Journal of Science & Technology, Transaction B: Engineering*, Vol. 34, pp. 471-485.
2. Mirzaei, M. & Sohankar, A. (2013). Heat transfer augmentation in plate finned tube heat exchangers with vortex generators: a comparison of round and flat tubes. *Iranian Journal of Science & Technology, Transactions of Mechanical Engineering*, Vol. 37, pp. 39-51.
3. Kays, W. & London, A. (1950). Heat transfer and flow friction characteristics of some compact heat exchanger surfaces. *Trans. ASME,* Vol. 72, pp. 1075-1097.
4. Chang, Y. J. & Wang, C. C. (1997). A generalized heat transfer correlation for Iouver fin geometry. *International Journal of Heat and Mass Transfer,* Vol. 40, pp. 533-544.
5. Beauvais, F. (1965). An aerodynamic look at automotive radiators. SAE Technical Paper.
6. Davenport, C. (1983). Correlation for heat transfer and flow friction characteristics of louvered fin. *AIChE Symp. Ser*, pp. 19-27.
7. Zhang, X. & Tafti, D. K. (2003). Flow efficiency in multi-louvered fins. *International Journal of Heat and Mass Transfer*, Vol. 46, pp. 1737-1750.
8. Webb, R. L. & Trauger, P. (1991). How structure in the louvered fin heat exchanger geometry. *Experimental Thermal and Fluid Science,* Vol. 4, pp. 205-217.
9. Zhang, X. & Tafti, D. K. (2001). Classification and effects of thermal wakes on heat transfer in multilouvered fins. *International Journal of Heat and Mass Transfer,* Vol. 44, pp. 2461-2473.

10. Zhang, L. W., Balachandar, S., Tafti, D. K. & Najjar, F. M. (1997). Heat transfer enhancement mechanisms in inline and staggered parallel-plate fin heat exchangers. *International Journal of Heat and Mass Transfer*, Vol. 40, pp. 2307-2325.
11. Zhang, L. W., Tafti, D. K., Najjar, F. M. & Balachandar, S. (1997). Computations of flow and heat transfer in parallel-plate fin heat exchangers on the CM-5: effects of flow unsteadiness and three-dimensionality. *International Journal of Heat and Mass Transfer*, Vol. 40, pp. 1325-1341.
12. Tafti, D. K. (1999). Time-dependent calculation procedure for fully developed and developing flow and heat transfer in louvered fin geometries. *Numerical Heat Transfer, Part A: Applications*, Vol. 35, pp. 225-249.
13. Tafti, D. K., Wang, G. & Lin, W. (2000). Flow transition in a multilouvered fin array. *International Journal of Heat and Mass Transfer*, Vol. 43, pp. 901-919.
14. Afanasyev, V. N., Chudnovsky, Y. P., Leontiev, A. I. & Roganov, P. S. (1993). Turbulent flow friction and heat transfer characteristics for spherical cavities on a flat plate. *Experimental Thermal and Fluid Science*, Vol. 7, pp. 1-8.
15. Ligrani, P. M., Mahmood, G. I., Harrison, J. L., Clayton, C. M. & Nelson, D. L. (2001). Flow structure and local Nusselt number variations in a channel with dimples and protrusions on opposite walls. *International Journal of Heat and Mass Transfer*, Vol. 44, pp. 4413-4425.
16. Ligrani, P. M., Burgess, N. K. & Won, S. Y. (2004). Nusselt numbers and flow structure on and above a shallow dimpled surface within a channel including effects of inlet turbulence intensity level. *Journal of Turbomachinery*, Vol. 127, pp. 321-330.
17. Sohankar, A. (2004). The LES and DNS simulations of heat transfer and fluid flow in a plate-fin heat exchanger with vortex generators. *Iranian Journal of Science and Technology*, Vol. 28, pp. 443-452.
18. Zhengyi, W., Khoon Seng, Y. & Boo Cheong, K. (2003). Numerical simulation of laminar channel flow over dimpled surface. *16th AIAA Computational Fluid Dynamics Conference*, ed: American Institute of Aeronautics and Astronautics.
19. Patrick, W. V. & Tafti, D. K. (2004). Computations of flow structure and heat transfer in a dimpled channel at low to moderate Reynolds number. *ASME 2004 Heat Transfer/Fluids Engineering Summer Conference*, pp. 401-412.
20. DeJong, N. C. & Jacobi, A. M. (2003). Localized flow and heat transfer interactions in louvered-fin arrays. *International Journal of Heat and Mass Transfer*, Vol. 46, pp. 443-455.
21. Kline, S. J. & McClintock, F. (1953). Describing uncertainties in single-sample experiments. *Mechanical engineering*, Vol. 75, pp. 3-8.